Available online at www.sciencedirect.com
SCIENCE DIRECT
Cement and Concrete Research 36 (2006) 330 – 336
Cement and Concrete Research

Three-dimensional visualization of pore structure in hardened cement paste by the gallium intrusion technique

Kiyofumi Kurumisawa [a,*], Kyoji Tanaka [b]

[a] Hokkaido University, Graduate School of Engineering, Nishi 8, Kita 13, Kita-ku, Sapporo, Hokkaido 060-8628, Japan
[b] Tokyo Institute of Technology, Structural Engineering Research Center, 4259 Nagatuta, Midori-ku, Yokohama, Kanagawa 226-8503, Japan

Received 12 May 2004; accepted 3 April 2005

Abstract

It is widely known that the pore structure of concrete strongly influences its physical properties. Therefore, we developed a technique for the visualization of the pore structure because of clearing it correctly. However, this visualization is limited to two-dimensional imaging for sections of the specimen. As a result, in this study, we developed a technique for reconstructing the acquired 2D images of the pore structure into 3D form by stacking them. By using this image, the relationship between water permeability and pore connectivity was clarified, and it was shown clearly that the pore connectivity strongly affects the water permeability.

Keywords: Microstructure (B); Image analysis (B); Cement paste (D); Gallium; Electron probe micro analysis (EPMA)

1. Introduction

The pore structure of concrete greatly influences its properties, particularly with respect to permeability and strength [1]. It is important to take the pore network into account while considering permeability. The pore network can be measured by mercury intrusion porosimetry (MIP); however, MIP cannot indicate the pore shape or the positions of the pores, which are important for analysing the pore connectivity [2–7]. Recently, the X-ray CT method [8] was proposed for analysing the properties of cement-based materials. However, this method cannot accurately indicate the pore structure because it is limited to areas of several square micrometers. In addition, Wood's metal intrusion [9,10] was employed for observing the pore structure clearly. This method provides clear two-dimensional images of the pores. In addition, we developed a technique for the visualization of the pore structure [11]. In this technique, which is based on MIP, we substituted gallium for mercury. Gallium intruded into the pores is observed in the solid phase by electron probe micro analysis (EPMA); this is carried out at room temperature because the melting point of gallium is 29.8 °C. Further, this observation was also limited to two-dimensional imaging for sections of the specimen. Owing to the 3D distribution of pores in cement-based materials, it was necessary to acquire 3D information relating to the correct pore shape and the distribution of pores. Therefore, several polishing operations

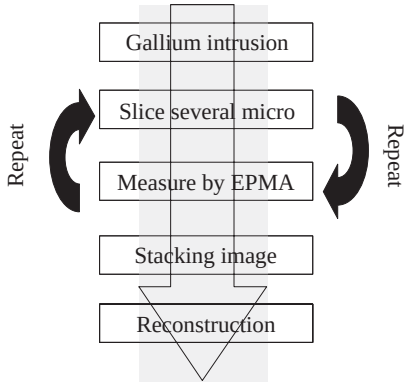

Fig. 1. Measuring procedure for 3D image of pore structure.

* Corresponding author. Tel.: +81 11 706 6306; fax: +81 11 706 7274.
E-mail address: kurumi@eng.hokudai.ac.jp (K. Kurumisawa).

0008-8846/$ - see front matter © 2005 Elsevier Ltd. All rights reserved.
doi:10.1016/j.cemconres.2005.04.015

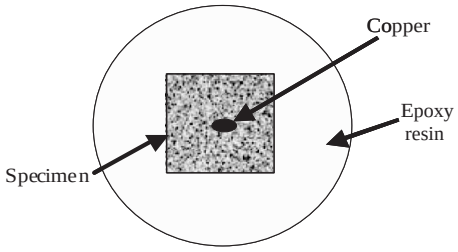

Fig. 2. Shape of specimen.

for the surface of the specimens of several square micrometers and observations by EPMA were performed. Three-dimensional images of the pore structure were reconstructed by stacking the acquired images of the pore structure. The purpose of this study is to observe the 3D shape of the pore structure using this image and clarifying the relationship between water permeability and pore connectivity.

2. Experimental procedure

Fig. 1 outlines the procedure for measuring the 3D image of the pore structure. First, the sections of the specimen where gallium has intruded into the pores are observed by EPMA. Next, the intruded gallium is observed after polishing the surface of a specimen of several square micrometers. This operation is repeated several times in order to acquire an image size that meets the required target size. Finally, the acquired images are appropriately stacked and reconstructed into 3D pore images.

2.1. Mixing, casting, and curing

Cement pastes with different water–cement ratios (W/C=0.45, 0.6) were employed as hardened cement specimens. The type of cement used was ordinary Portland cement, which was mixed with distilled water. The mould of a cylinder having a diameter and depth of 100 and 30 mm, respectively, was created. After a day, the specimens were demoulded followed by water curing for 7 to 28 days at 20 °C. In order to observe the specimen in the same position every time, compressed copper with a diameter of 0.08 mm was used as the target by inserting it in every specimen observed, as shown in Fig. 2.

2.2. Sample preparation

2.2.1. Cutting of sample and preparation before intrusion

Cubic test pieces with a side length of approximately 5 mm were cut from around the centres of the specimens using a diamond cutter and washed with acetone to eliminate hydration. The specimens were then dried by D-dry (specimens in desiccator under 0.065 Pa using a vacuum pump and dry ice) for 48 h to remove moisture in the pores.

2.2.2. Intrusion of gallium

In each specimen, gallium was intruded into and fixed in the pores. Theoretically, a maximum pressure of 150 MPa should enable the intrusion of gallium into the pores with a diameter of 5 nm.

2.3. Preparation of samples for EPMA measurement

After the intrusion process, gallium on the surface of the sample was thoroughly removed. The sample was placed in a mould with a diameter and depth of 25 and 20 mm, respectively, and the space around the sample was filled with epoxy resin. After the resin was cured, the mould was removed and its surface was polished progressively using polishing paper. The polishing was carried out using a 0.25-μm diamond slurry. The specimen was then subjected to ultrasonic cleaning. The sample was simultaneously cooled during polishing in order to prevent melting of the gallium. The surface was then coated with platinum in order to impart conductivity. Next, the EPMA was applied to the specimen in the same position using the inserted copper as the target. Since the pore structure around the copper appeared to be coarse, a sampling area away from the copper by approximately 100 μm was chosen. In this study, the sampling area was 150 μm^2, as shown in Fig. 3. In this

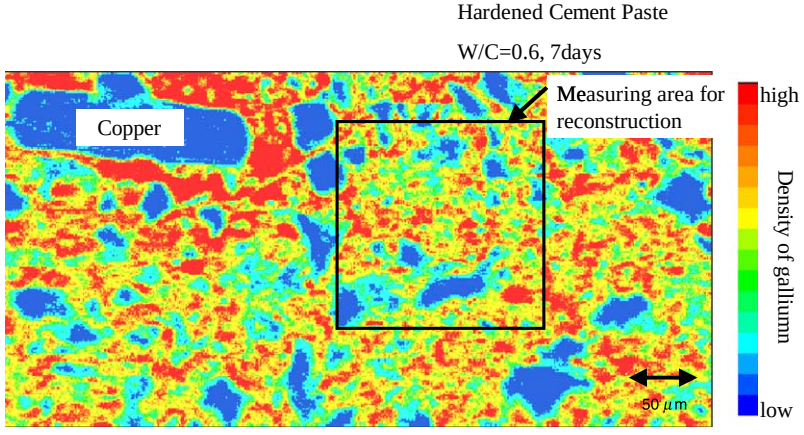

Fig. 3. Sampling position for EPMA measurement.

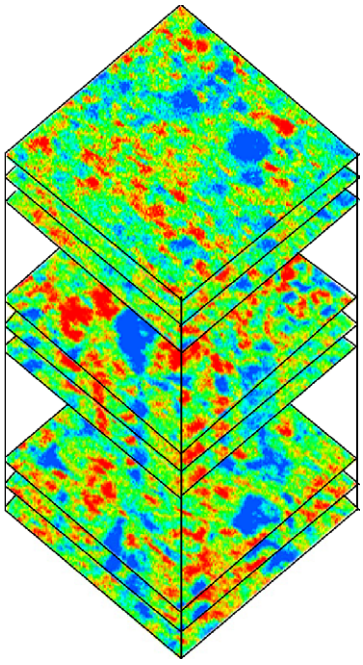

Fig. 4. Stacking 2D images.

figure, a red pixel indicates a high density of gallium while a blue pixel indicates a low density of gallium. Gallium was used as the measuring element in the EPMA, and the measurement was carried out for every 1-μm movement of the specimen surface. For the stacking of the 2D images, the surface of the specimen was polished to remove several microns using a diamond paste of 1 μm, and the thickness of the specimen was measured using a dial gauge after each EPMA measurement. Fig. 4 shows the stacking procedure of the 2D pore images. In this study, the polished thickness was approximately 2 μm.

3. Results

3.1. Shape of the 3D pore structure

The image of the 3D pore of the hardened cement paste is shown in Fig. 5. The pixel colour approaches red as the concentration of gallium per square micrometer increases, while it approaches blue as the concentration decreases. The red pixels indicate that the entire 1-μm^2 area is composed of gallium, which shows that the entire pixellated area represents a pore, while the pixels in blue indicate the solid phase. Further, it was assumed that the degree of porosity could be represented in terms with the concentration of gallium as a reference. The result for the section of the specimen at the centre is shown in Fig. 6. The form of the internal pores can be identified by this method.

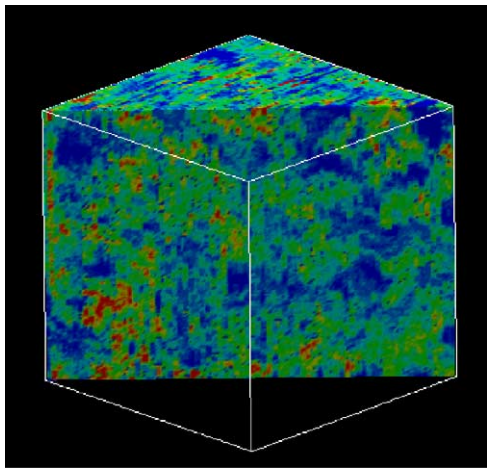

Fig. 6. The pore structure in section of specimen.

3.1.1. Effect of W/C ratio

A 7-day old specimen with $W/C=0.6$ is shown Fig. 5, while a 7-day old specimen with $W/C=0.45$ is shown in Fig. 7. The specimen with $W/C=0.45$ has many low-concentration areas. On the other hand, the specimen with $W/C=0.6$ has many high-concentration areas. Therefore, specimens with a low water-to-cement ratio have a dense structure with many low-concentration areas, whereas specimens with a higher water-to-cement ratio have a coarse structure with many high-concentration areas.

3.1.2. Effect of curing age

The 7-day old specimen with $W/C=0.45$ is shown in Fig. 7, and the 28-day old specimen is shown in Fig. 8. The

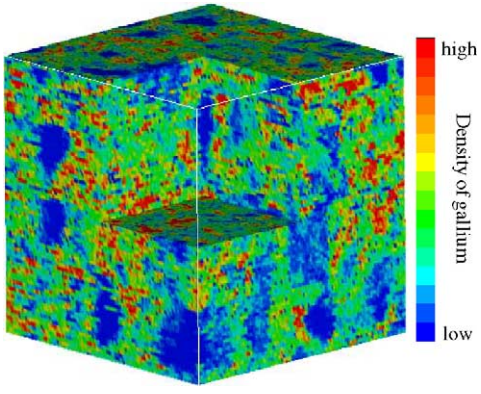

Fig. 5. 3D image of pore structure ($W/C=0.6$, 7 day).

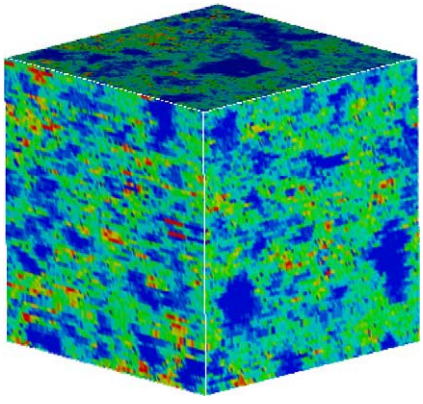

Fig. 7. 3D image of pore structure ($W/C=0.45$, 7 day).

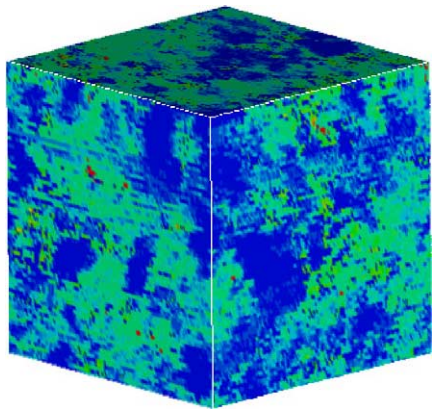

Fig. 8. 3D image of pore structure ($W/C=0.45$, 28 day).

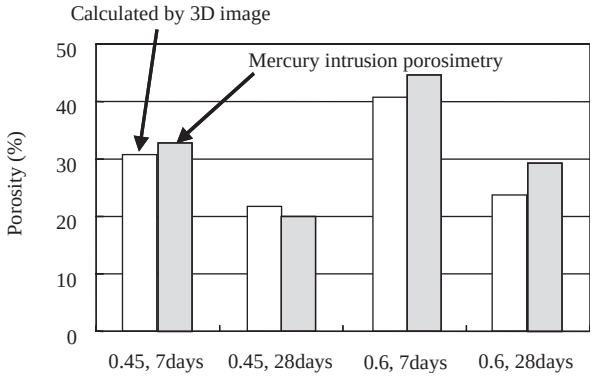

Fig. 10. Comparison of porosity with various methods.

28-day old specimen has many low-concentration areas, while the 7-day old specimen has many high-concentration areas. This indicates that a specimen at early age has a coarse structure with many high-concentration areas, whereas the pore structure in hardened cement paste becomes denser with an increase in curing age.

3.1.3. Pores in the specimen with a diameter exceeding 1 μm

Since it is possible to identify areas with the pore diameter exceeding 1 μm in the specimen by EPMA, only a portion of such an area is shown in Fig. 9. The left-hand side of the figure shows $W/C=0.6$ after 7 days, and the figure at the right-hand side shows $W/C=0.6$ after 28 days. The white portion represents pores over 1 μm. Further, this white portion can be clearly observed for 7 days. However, after 28 days, the white portion is barely visible, which indicates that the pores over 1 μm hardly exist. Hence, the specimen at 7 days has many pores, which indicates that the pore connectivity might be high. Moreover, the number of pores decreased considerably with increasing curing age.

3.2. Comparison of porosity using pore image and MIP

The porosities calculated by the pore image and that obtained by MIP were compared. The method of calculating porosity from the image is explained briefly in this study (described in detail in a previous report [11]). Since the measured image was expressed as a function of concentration, the porosity was calculated under the assumption that the porosity of 1 μm^2 changes for each concentration followed by its integration. This result is shown in Fig. 10. The result calculated from the 3D image was almost the same as that obtained from the mercury intrusion method. Therefore, when measuring porosity, the 3D image proves to be useful.

4. Discussion of pore connectivity

4.1. Assumption of pores

Pore connectivity affects substance penetration in concrete to a great extent. Therefore, it is important to understand the pore connectivity three dimensionally. For the pixels in which the gallium concentration exceeded a certain threshold, as shown in Fig. 11, the entire pixel was assumed to represent the pore structure. For pixels below the threshold value, the pixel was assumed to represent the solid phase. An example of the obtained image that contains four cases of the threshold (0.1, 0.5, 0.8, and

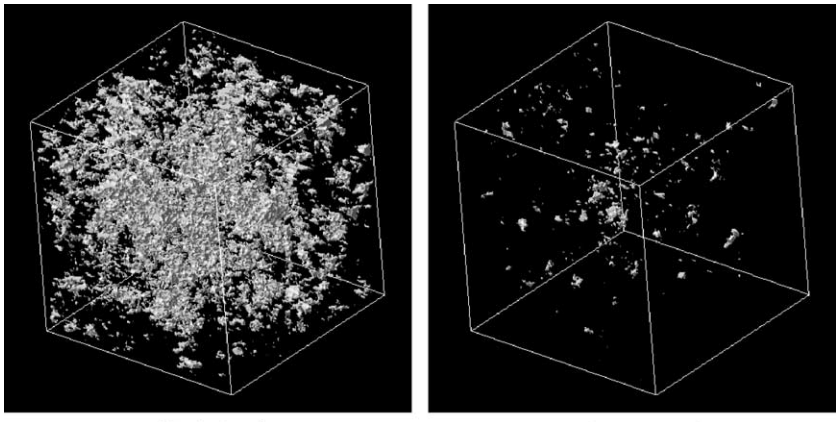

Fig. 9. Pores over 1 μm in specimen (the white portion indicates pores).

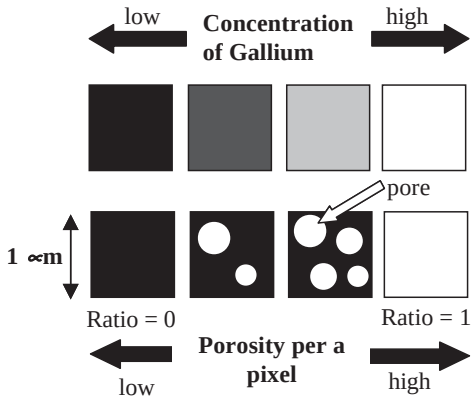

Fig. 11. Threshold of pore image.

1.0) is shown in Fig. 12. In this figure, the white portion represents the pore phase and the black portion represents the solid phase. In order to calculate the connectivity of the pores, a pixel which is greater than a certain threshold was assumed as a pore. The connectivity of the pores can be examined by establishing a certain threshold and performing binary processing. The occupation of three-dimensional pore pixels in each specimen at the case of threshold change (assumed porosity per pixel), considered as binary images, is calculated, and the result is shown in Fig. 13. The occupation rate (assumed porosity) represents the rate at which the pore pixel (white portion) occupies the pore throughout the entire specimen at a certain threshold. When the threshold decreases, the number of pore pixels increases and the assumed porosity increases as well. For example, when the threshold value is 0.1, as shown in Fig. 12, many pores exist, which leads to an increase in the assumed porosity. Moreover, irrespective of the threshold, it can be observed from this figure that the porosity in each specimen increases with a high water-to-cement ratio and at an early curing age.

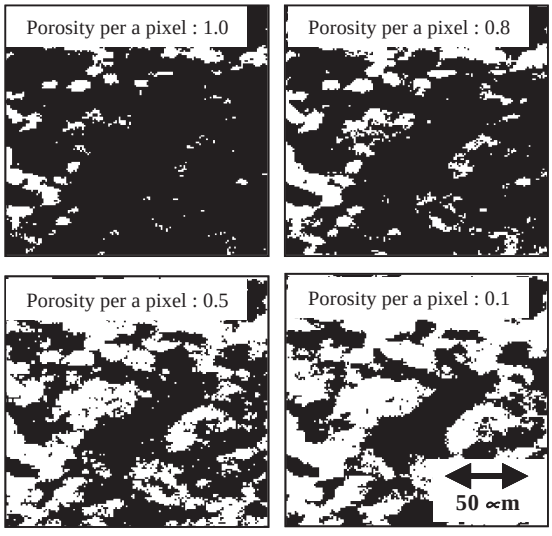

Fig. 12. Porosity per pixel in pore image.

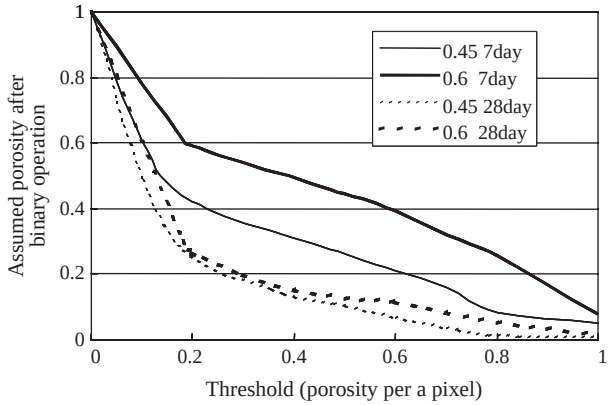

Fig. 13. Relation between assumed porosity and threshold (porosity per pixel).

4.2. Evaluation of pore connectivity

The connectivity of a pore is evaluated by the connected pore pixels in the specimen from the top to the bottom side. The connectivity is expressed using the following formula:

Pore connectivity

$$= (\textit{Number of connected pixels of the pore from the top to bottom})/(\textit{Number of pixels of the pores in the specimen}).$$

An index of 1 implies that all the pore pixels are connected. An index of 0 indicates that no pore pixels are connected. This implies that when the index has a high value, a substance can easily penetrate the specimen. Conversely, penetration is difficult when the index is 0.

4.3. Relationship between porosity and pore connectivity

The relationship between the assumed porosity in each specimen after the binary operation and the pore connectivity is shown in Fig. 14. When the pore connectivity is zero, which indicates a complete lack of connectivity, the overall porosity of a specimen is lower than 0.05. Regardless of the pore distribution, when the porosity of the

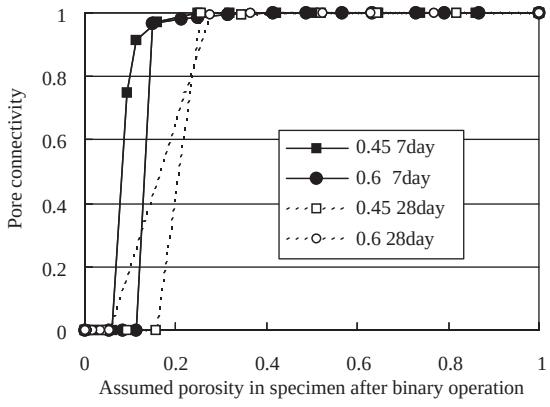

Fig. 14. Relation between porosity and pore connectivity.

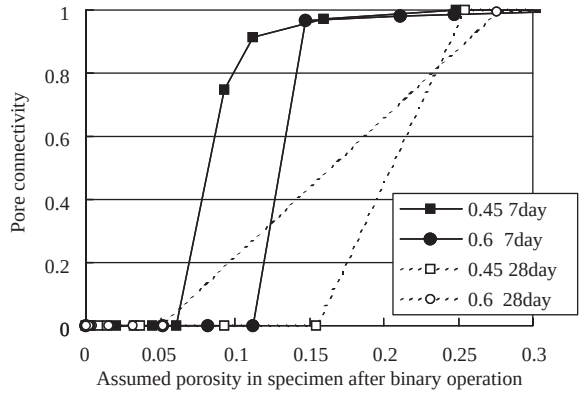

Fig. 15. Relation between porosity and pore connectivity (range 0–0.3).

specimen becomes lower than 0.2, it is difficult for a substance to penetrate in the specimen (Bentz and Garboczi [12]).

The pore connectivity of the C_3S paste is reported to be zero below a capillary porosity of 0.2 under different W/C ratios from the simulation of a cement hydration model. However, in this study, the difference in the pore connectivity between the specimens is shown in Fig. 14, and it is considered to be based on the difference in their pore structure. The difference in the pore connectivity near the threshold (0–0.3) is shown in Fig. 15. Different specimens have different pore connectivity at the same porosity. Ye [13] investigated the relationship between the permeability and the porosity of hardened cement paste under different W/C and curing periods and reported that the relationship between the porosity and permeability is not unique.

4.4. Relationship between pore connectivity and threshold (assumption porosity per pixel)

The results of the calculation of the pore connectivity for each threshold (assumption porosity per pixel) are shown in Fig. 16. When the threshold is 1, the pore connectivity in all the specimens was observed to be zero, indicating a lack of connectivity. However, when the threshold is less than 1, the connectivity acquires an extremely high value. For example,

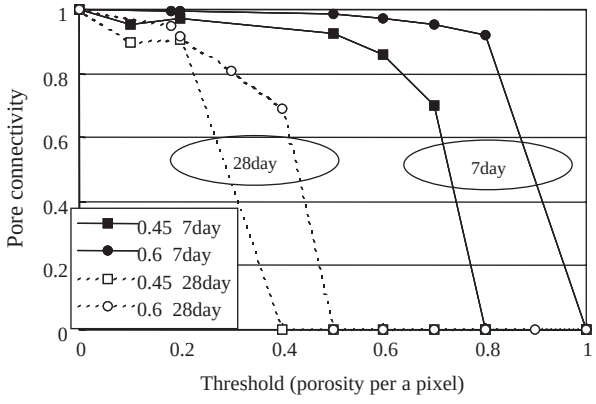

Fig. 16. Relation between pore connectivity and threshold (porosity per pixel).

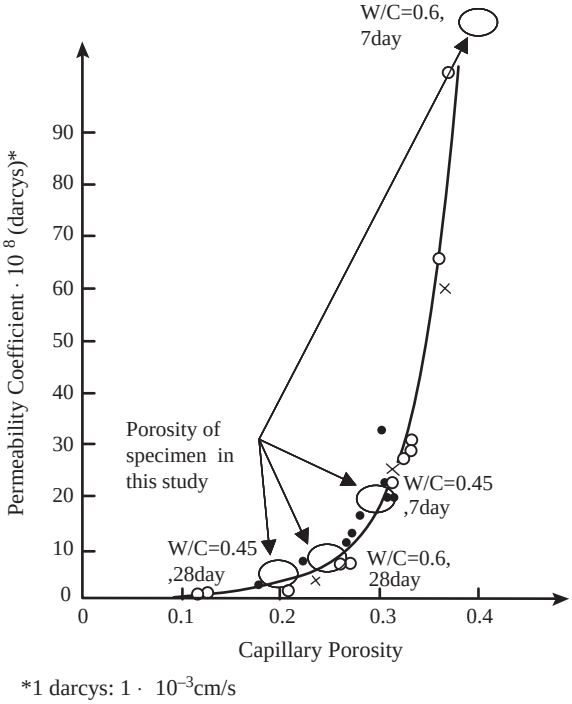

Fig. 17. Permeability coefficient in this study [1].

the connected pores are observed in a specimen of $W/C=0.6$ at 7 days; however, the threshold value is 1. In the case of the 28-day old specimens, the pore connectivity is zero in a low threshold range. On the contrary, the pore connectivity of the 7-day old specimens is zero in high threshold range. Thus, for different ages, the pore connectivity changes with the threshold in a peculiar manner. This tendency is also observed in the case of different water-to-cement ratios. When this ratio is high, the pore connectivity is 0 at a high threshold. Conversely, the pore connectivity with a low water-to-cement ratio is 0 at a low threshold. It is considered that the specimens at an early age or with a high water-to-cement ratio have high connectivity due to the large amount of interconnected pores. Therefore, substances such as chloride ion and carbon dioxide are easily penetrated into these cement-based materials.

4.5. Relationship between permeability and pore connectivity

The relationship between the pore connectivity and permeability is investigated. In this study, the value of the permeability coefficient of the porosity and the corresponding result reported by Powers [1] is shown in Fig. 17. In this

Table 1
Permeability coefficient in this study

	0.45, 28 day	0.6, 28 day	0.45, 7 day	0.6, 7 day
Permeability coefficient ($\times 10^8$ darcy)	3	6	20	120

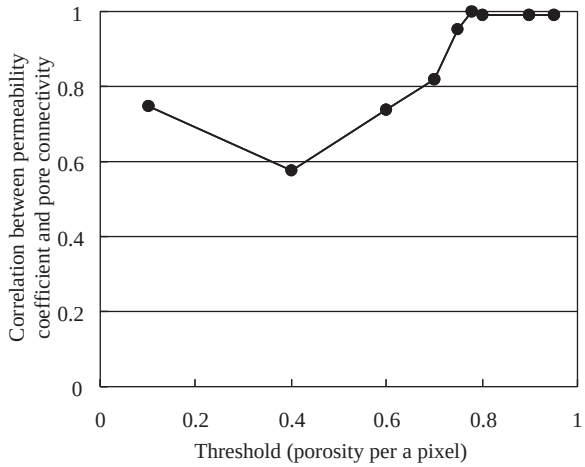

Fig. 18. Relation between correlation coefficient and threshold.

case, the value of the permeability coefficient is shown in Table 1. A comparison of the result obtained from the permeability examination by T. C. Powers with the relationship of the pore connectivity (Fig. 14) is performed. The pore connectivity decreases in all the specimens when the porosity is 0.2 or less, as shown in Fig. 14. In the result of T.C. Powers, the permeability coefficient is quite low at a porosity of 0.2 or less. Moreover, when the porosity is 0.2 or more, the pore connectivity significantly increases and the permeability coefficient also increases to an extremely large value. This result indicates that in this study, the pore connectivity and the water permeability are closely related.

When the pore connectivity is assumed as an index for evaluating the permeability of cement-based material, the significant influence of the threshold (assuming porosity per pixel) on the permeability was examined. The correlation of the pore connectivity and the permeability coefficient is also investigated, and this is shown in Fig. 18. When the threshold (porosity per pixel) is set to approximately 0.8, the correlation with the permeability coefficient and the pore connectivity becomes high. As a result, thresholds having a value of 0.8 or more are considered to have a considerable influence on the water permeability coefficient, i.e., the connectivity of the comparatively larger pores is considered to affect the water permeability. This result corresponds with past research [14,15].

Therefore, the size and volume of the pores are important factors in influencing the permeability; however, the pore connectivity assumed in this paper is considered to have a considerable effect on permeability.

5. Conclusion

The following conclusions were obtained from this study:

1) The measurement procedure in this study can reconstruct the three-dimensional image of the pore structure in hardened cement paste by stacking two-dimensional pore structure images acquired by EPMA.
2) The 3D pore image varies with the W/C ratio and the curing age. Further, the network of the pores with a diameter greater than 1 μm has been clarified by the proposed method.
3) Since the porosity calculated by this method is similar to the result determined by MIP, this method can estimate the porosity and reveal the shapes of the pores.
4) An index by which the pore connectivity can be evaluated on the basis of the pore structure of a hardened cement paste that has been three-dimensionally reconstructed is proposed. The pore conductivity is closely related to the water permeability.

References

[1] T.C. Powers, Structure and physical properties of hardened Portland cement paste, J. Am. Ceram. Soc. 41 (1) (1958) 1–6.
[2] W. Hansen, J. Almudaiheem, Pore structure of hydrated Portland cement measured by nitrogen sorption and mercury intrusion porosimetry, Microstructure Development During Hydration of Cement, Materials Research Society, 1986, pp. 105–114.
[3] P.W. Brown, D. Shi, Porosity/Permeability Relationships, Materials Science of Concretell, American Ceramic Society, 1991, pp. 83–109.
[4] R.A. Cook, K.C. Hover, Mercury porosimetry of hardened cement paste, Cem. Concr. Res. 29 (6) (1999) 933–943.
[5] D.N. Winslow, D. Liu, The pore structure of paste in concrete, Cem. Concr. Res. 20 (2) (1990) 227–235.
[6] Y.W. Mai, B. Cotterell, Porosity and mechanical properties of cement mortar, Cem. Concr. Res. 15 (6) (1985) 995–1002.
[7] D.N. Winslow, C.W. Lovell, Measurements of pore size distributions in cements, aggregates and soils, Powder Technol. 29 (1981) 151–165.
[8] H. Uchikawa, S. Uchida, S. Hanehara, Measuring method of pore structure in hardened cement paste, Mortar Concr., il Cemento 88 (1991) 67–90.
[9] A.B. Abell, K.L. Willis, D.A. Lange, Mercury intrusion porosimetry and image analysis of cement-based materials, J. Colloid Interface Sci. 211 (1) (1999) 39–44.
[10] K.L. Willis, A.B. Abell, D.A. Lange, Image-based characterization of cement pore structure using wood's metal intrusion, Cem. Concr. Res. 28 (12) (1998) 1695–1705.
[11] K. Tanaka, K. Kurumisawa, Development of technique for observing pores in hardened cement paste, Cem. Concr. Res. 32 (9) (2002) 1435–1441.
[12] D.P. Bentz, E.J. Garboczi, Percolation of phases in a three-dimensional cement paste microstructural model, Cem. Concr. Res. 21 (2) (1991) 325–344.
[13] G. Ye, Percolation of capillary pores in hardening cement pastes, Cem. Concr. Res. 35 (1) (2005) 167–176.
[14] S. Goto, D.M. Roy, The effect of W/C ratio and curing temperature on the permeability of hardened cement paste, Cem. Concr. Res. 11 (4) (1981) 575–579.
[15] J. Holly, D. Hampton, M.D.A. Thomas, Modelling relationships between permeability and cement paste pore microstructures, Cem. Concr. Res. 23 (6) (1993) 1317–1330.